Anderson localization of light in dimension $d - 1$

Carlos E. Máximo,[1] Noel A. Moreira,[2,3] Robin Kaiser,[3] and Romain Bachelard[1,3]

[1]*Departamento de Física, Universidade Federal de São Carlos, Rod. Washington Luís, km 235 - SP-310, 13565-905 São Carlos, SP, Brazil*
[2]*Instituto de Física de São Carlos, Universidade de São Paulo - 13560-970 São Carlos, SP, Brazil*
[3]*Université Côte d'Azur, CNRS, INPHYNI, F-06560 Valbonne, France*

Localization of electromagnetic waves in disordered potentials is prevented by polarization terms, so only light-scattering systems of dimensions $d = 1$ and 2 with scalar properties exhibit light localization. We discuss here the presence of surface modes in vectorial systems of dimensions $d = 2$ and 3, which possess lower-dimensional scattering properties, and present features of Anderson localization. In particular, vectorial waves in three dimensions (two dimensions) presents surface localized modes with scaling consistent with localization in two dimensions (one dimension).

I. INTRODUCTION

Introduced in the context of electronic transport by Anderson [1], the localization of waves in a disordered potential was later understood to be a general wave phenomenon. Acoustic [2,3], matter [4–7], surface-plasmon polaritons [8], or electromagnetic waves [9–16] were shown to localize as well, and the universal "scaling analysis" [17], which does not account for the microscopic details, suggested that the only critical parameter was the dimension: one- and two-dimensional (1*D* and 2*D*) systems from the orthogonal symmetry class always present localization features, being hindered only by the finite system size. In contrast, three-dimensional systems localize above a critical disorder.

A shadow was cast on this universal picture when it was discovered that the vectorial character of electromagnetic waves prevents localization [18,19]. Initially discussed for three-dimensional (3*D*) systems, for which the conclusions of experimental reports had been already questioned [12,13,20,21], a similar result was reported for two-dimensional light scattering [22]: In-plane polarizations, which are coupled to each other, present vectorial properties and do not localize, whereas the polarization orthogonal to the plane, uncoupled from the others, behaves as a scalar wave and exhibits localized modes [23]. This situation now calls for an experimental verification of the role of polarization, as it was, for example, proposed in Ref. [24] by imposing a strong magnetic field to decouple the different scattering channels.

From a theoretical point of view, the scaling theory of localization, which focuses on the thermodynamic limit, has been recognized as the standard method to demonstrate the transition to localization in any type physical systems. Nevertheless, it does not take into account finite-size phenomena that arise at the boundaries of the samples. In this paper, we show that the presence of surface modes in homogeneous samples leads to the emergence of Anderson-localized modes at the surface of vectorial-wave systems. More specifically, vectorial electromagnetic waves in dimensions $d = 2$ and 3 present scattering modes with exponentially decaying profiles

along the surface, with localization lengths that scale as the mean-free path in dimensions $d = 1$ and 2.

Studies of Anderson localization of light waves usually consider distributions prone to surface modes, i.e., with homogeneous densities (to yield homogeneous localization properties) and high densities (to reach strongly scattering samples). Anderson localization *a priori* refers to the thermodynamics limit of infinite samples, where the proportion of surface modes vanishes. Nevertheless, these localized surface modes for vectorial waves may still be very relevant since, on the one hand, the samples used to study Anderson localization are usually rather small in terms of optical wavelengths and, on the other hand, they correspond to the boundary between the scattering medium and the surrounding one.

In the next section, we present the microscopic model used to describe the light scattering in dimensions 2 and 3. In Sec. III, we present our analysis, as well as the localization at the surface of 2*D* systems. In Sec. IV, these results are extended to 3*D* systems. Finally, in Sec. V we draw our conclusions and discuss the perspective for surface localization.

II. POINT-SCATTERER MODEL

To address the vectorial light-scattering problem in dimensions $d = 2$ and 3, we use a microscopic model that describes N point-like two-level dipoles, with positions $\mathbf{r}_j$, coupled through the vacuum modes of the d-dimensional space. In the linear optics regime, the formal Markovian integration of the vacuum-mode dynamics yields the following effective interactions between pairs of dipoles [22,25,26]:

$$K^{2D}_{\alpha\beta}(\mathbf{r}_{jl}) = \delta_{jl}\delta_{\alpha\beta} + (1 - \delta_{jl})[\delta_{\alpha\beta}H_0(kr_{jl})$$
$$+ (1 - \delta_{\alpha\beta})e^{2\alpha i\phi_{jl}}H_2(kr_{jl})], \quad (1)$$

$$K^{3D}_{\alpha\beta}(\mathbf{r}_{jl}) = \delta_{jl}\delta_{\alpha\beta} + (1 - \delta_{jl})[\delta_{\alpha\beta}f(kr_{jl})$$
$$+ \mathcal{D}_{\alpha\beta}(\hat{\mathbf{r}}_{jl})g(kr_{jl})], \quad (2)$$

where the polarization components are $\alpha, \beta = \pm 1$ for $2D$ and $\alpha, \beta = 0, \pm 1$ for $3D$. H_n is the Hankel function of the first kind and of order n, and $r_{jl} = \|\mathbf{r}_{jl}\|$ is the Euclidean distance in a given dimension, with $\mathbf{r}_{jl} \equiv \mathbf{r}_j - \mathbf{r}_l$. Furthermore, $\hat{\mathbf{r}}_{jl} = \mathbf{r}_{jl}/r_{jl}$ represents the unitary vector

$$\hat{\mathbf{r}}_{jl} = \begin{cases} (\cos \varphi_{jl}, \sin \varphi_{jl}) & \text{for } d = 2 \\ (\sin \theta_{jl} \cos \varphi_{jl}, \sin \theta_{jl} \sin \varphi_{jl}, \cos \theta_{jl}) & \text{for } d = 3. \end{cases} \tag{3}$$

Finally, we introduce the functions

$$f(x) = \frac{3}{2} \frac{e^{ix}}{ix} \left(1 - \frac{1}{x^2} + \frac{i}{x} \right),$$

$$g(x) = \frac{3}{2} \frac{e^{ix}}{ix} \left(\frac{3}{x^2} - \frac{3i}{x} - 1 \right), \tag{4}$$

$$\mathcal{D}_{\alpha\beta}(\hat{\mathbf{r}}_{jl}) = (-1)^{\delta_{\alpha\beta}+1} e^{i(\beta-\alpha)\varphi_{jl}} \cos^2 \theta_{jl} \left(\frac{\tan \theta_{jl}}{\sqrt{2}} \right)^{|\alpha|+|\beta|}.$$

The resulting collective scattering modes are given by the eigenvectors Φ of the non-Hermitian Green's matrices (1) and (2) [18,27]. Note that, in the present form, these matrices describe the resonant scattering by two-level systems, with a unitary linewidth and a resonant energy arbitrarily fixed to zero. Thus, the imaginary part of their eigenvalue associated with each mode corresponds to their shift in energy relative to this resonance, which can be selected by appropriately tuning the frequency of the driving light [28].

In two dimensions, the vectorial nature of the scattering manifests itself in Eq. (1) through the near-field term H_2, which is known to suppress exponentially localized modes over the sample area [22]. Such a term is absent in the two-dimensional scalar model, in which all features of Anderson localization persist [15,22,23]. Similarly, a scalar light approximation can be performed in three dimensions, where the polarization term $\mathcal{D}_{\alpha\beta}$ is neglected and only the leading order in f for $r \gg 1$ is kept. While this scalar simplification induces a nonphysical transition to localization, the full $3D$ vectorial model predicts an absence of transition [18,19]. For this reason, throughout this work we focus on the vectorial models, which are not expected to present any localized modes.

Here, we consider random distributions $\mathbf{r}_j$ with homogeneous densities ρ_d. This corresponds, for instance, to the case of white paint samples [14,16] or macroporous GaP samples [13]. This is also the approach adopted by theorists, because the localization properties depend on the disorder strength, which is here tuned through the scatterer density [29]. Furthermore, the existence of a critical disorder threshold to reach the localization transition in $3D$ requires strongly scattering samples. Considering an effective-medium point of view, highly scattering and homogeneous samples naturally lead to the emergence of surface modes [30].

III. METHODS AND SURFACE LOCALIZATION IN TWO DIMENSIONS

Once the disorder is accounted for, the surface modes, which possess the scattering properties of a medium of dimension $d - 1$, are candidates for Anderson localization. This
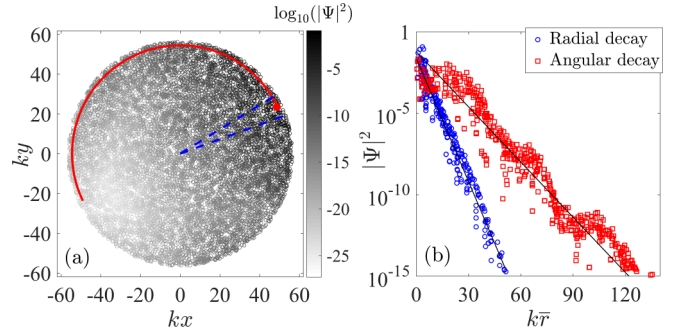
FIG. 1. (a) $2D$ profile of a surface Anderson-localized mode. The red line starts at the center of mass, and depicts the thin layer where the angular profile is computed, whereas the blue dashed lines delimit the slice where the radial profile is computed. (b) Spatial decay along the radial axis and along the surface (angular decay), with the black lines corresponding to the exponential fit. $\bar{r}$ refers to the radius r for the radial decay, and to $R\phi$, with R being the cloud radius. Simulations were realized for $N = 10^4$ scatterers and a density $\rho_2 = k^2$.

is illustrated in Fig. 1, where a surface Anderson-localized mode from the $2D$ vectorial model (1) is presented. A closer inspection reveals in Fig. 1(b) that there are two "localization" mechanisms, as can be expected from the above discussion. On the one hand, the radial confinement, visible from the exponential radial decay of

$$|\Psi_j|^2 = \sum_{\alpha=-1}^{+1} \left| \Phi_j^{(\alpha)} \right|^2, \tag{5}$$

originates in the high scatterer density; this mechanism is the same as for whispering-gallery modes, well described by Mie theory using the refractive index approach [31], and corresponds to a kind of Purcell effect, with increased scattering into the surface modes. On the other hand, Anderson localization manifests as an exponential decay of the mode amplitude along the surface [labeled "angular decay" in Fig. 1(b)] and is the result of the presence of disorder. Macroscopic oscillations can be observed in this angular decay profile, which we attribute to a resonance condition, where the whispering gallery mode must present an integer number of periods along the system boundary.

To identify surface modes, we first select the modes whose center of mass $|\mathbf{r}^{\text{c.m.}}|$ is at most at a distance $R/10$ from the surface, with R being the radius of the cloud. We observe that the closer to the surface, the more exponential-like is the decay of the mode profile. A skin depth δ_m of the mode m is then defined through the fitting $e^{-|\mathbf{r}_j - \mathbf{r}_m^{\text{c.m.}}|/\delta_m}$, performed over the atoms in a radial slice [see Fig. 1(a)]. We have chosen to consider modes as surface modes when the exponential fit yields a confidence level above 0.9 (using the coefficient of determination R^2). Then, we select the surface-localized modes by performing an angular fitting $e^{-R(\phi_j - \phi_m^{\text{c.m.}})/\xi_m}$ over the atoms in a layer δ_m, only for the surface modes, with $\phi^{\text{c.m.}}$ being the angular coordinate of the center of mass and ξ_m being the angular localization length [see Fig. 1(b)]. Using this protocol, the majority of surface modes (i.e., with an exponential radial decay from the surface) appear to be localized
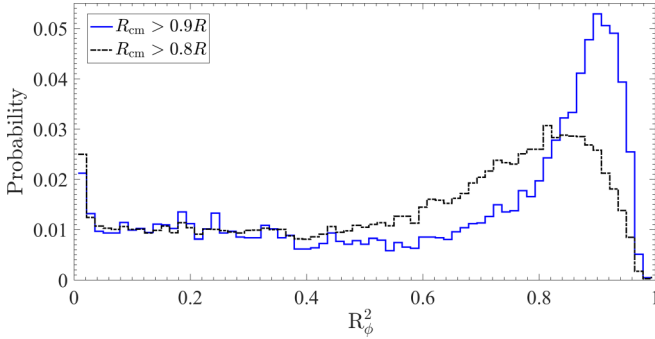
FIG. 2. Histogram of the R_ϕ^2 coefficient for the angular fit, using 70 regular bins and obtained for clouds with $\rho_2 = k^2$, $N = 4000$, using 21 realizations.

along the surface as well, with an exponential angular decay: This is illustrated in Fig. 2, where the histogram of the R_ϕ^2 fitting coefficient, for the angular profile, presents a stronger peak close to unity for modes closer to the surface.

Let us now analyze qualitatively these confining mechanisms. In dimension d, an effective medium approach for a homogeneous sample of scatterer density ρ_d predicts the presence of waves confined along the surface over a skin depth [32]

$$\delta_d \sim \mathrm{Re}(1/k\sqrt{n^2 - 1}), \qquad (6)$$

with n being the refractive index. This results in the surface modes propagating in a $(d-1)$-dimensional disordered medium whose effective scatterer density and mean-free path are given by

$$\rho_{d-1}^{\mathrm{s}} = \rho_d \delta_d, \qquad (7a)$$

$$l_{d-1}^{\mathrm{s}} = \frac{1}{\sigma_{d-1}\rho_{d-1}^{\mathrm{s}}}, \qquad (7b)$$

where $\sigma_d = 8/k$ here refers to the scattering cross section for scalar light in dimension $d = 2$ ($\sigma_d = 1$ for $d = 1$).

Let us first consider the two-dimensional case. Surface modes then propagate in a $d = 1$ space, where light is known to localize for any amount of disorder [33]. The localization length is then $\xi_1^{\mathrm{s}} \sim l_1^{\mathrm{s}} = 1/\sqrt{8\rho_2}$ since the refractive index at resonance is

$$n^2 = 1 + 4i\frac{\rho_2}{k^2}. \qquad (8)$$

This qualitative analysis is confirmed by direct numerical simulations, where the averaged localization length $\xi = \langle \xi_m \rangle$ and the skin depth $\delta = \langle \delta_m \rangle$ are extracted from exponential fits to the spatial decay of the surface modes: As can be seen in Fig. 3(a), the localization length of the surface modes scales with the 1D mean-free path l_1^{s}, but scales quite differently from both the 2D mean-free path l_2 and from the prediction of the self-consistent theory, which assumes a weak disorder [34,35]: $\xi_2^{\mathrm{wd}} = l_2\sqrt{\exp(\pi k l_2) - 1}$. Furthermore, even though the skin depth measured in the simulations and that predicted from Eq. (6) differ by a factor ~ 10, they present the predicted scaling $\delta_2 \sim 1/\sqrt{\rho_2}$. A possible source for this discrepancy is the fact that the skin depth (6) normally stands for the evanescent wave outside the medium, in addition to the fact
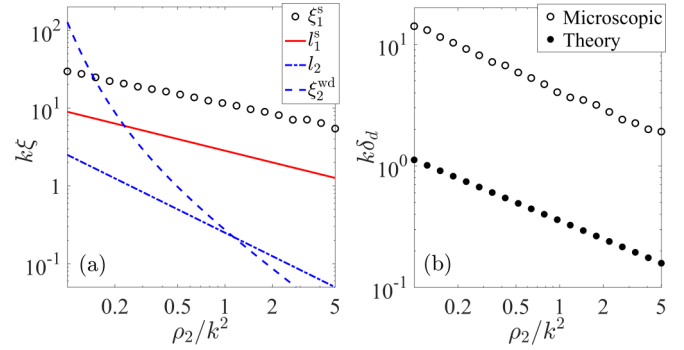
FIG. 3. (a) Localization length ξ_1^{s} and (b) skin depth δ_d of Anderson-localized surface modes, as a function of the sample density ρ_2, for the 2D vectorial scattering problem. It is compared with the 1D surface localization length l_1^{s} and with the 2D mean-free path l_2 and weak-disorder prediction ξ_2^{wd} (see main text for details). Simulations were realized for a cloud of $N = 10^4$ scatterers, where ξ is computed by using an average over all localized surface modes, and for a single realization for each value of density.

that Eq. (8) for the refractive index has a limited validity for high densities and close to resonance.

As the effective medium theory predicts no angular confinement (the scattering modes by a homogeneous dielectric are provided by the spherical harmonics in Mie theory [31]), the angular confinement is due to the disorder, i.e., Anderson localization. On the other hand, the difference in the radial and angular decay lengths shows that two distinct confining mechanisms are at play. We therefore attribute our findings to surface Anderson localization of light.

The presence of surface propagation must be associated with a strong modification of the local density of states (LDOS) close to the surface, which results in an anisotropic random walk of the photons between the scatterers. In particular, the LDOS of an effective-medium theory should capture the preferential emission along the surface, whereas applied to the microscopic model used in this work [36], it may allow us
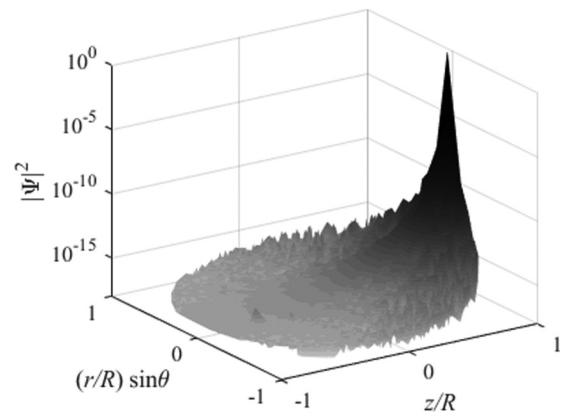
FIG. 4. Surface localized mode from the 3D vectorial model (2). The coordinates refer to spherical ones, with the z axis chosen to cross the mode center of mass. The color code refers to the mode distribution $|\Psi_j|^2$. Simulations were realized for a cloud of $N = 5000$ scatterers, with a density $\rho = 100k^3$.
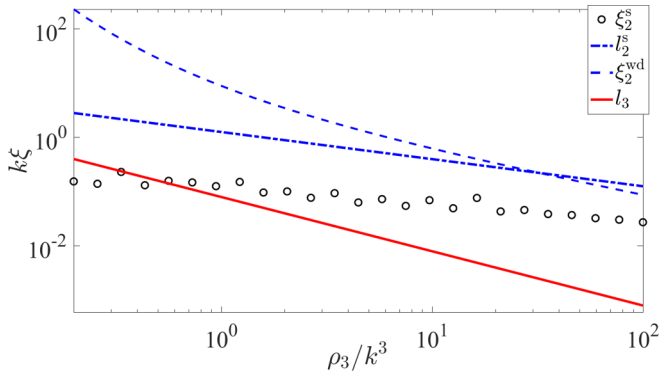
FIG. 5. Localization length ξ_2^s of the surface modes for the $3D$ vectorial model (2), compared with the $3D$ mean-free path l_3 and to the $2D$ scattering mean-free path l_2^s and weak-disorder prediction ξ_2^{wd} (see main text for details). Simulations realized for a cloud of $N = 5000$ scatterers, where ξ is computed by using an average over all localized surface modes, and for a single realization for each value of density.

to investigate in more detail the differences between the radial and superficial confinements.

IV. SURFACE LOCALIZATION IN THREE DIMENSIONS

In three dimensions, localization of light has been more elusive: Experimentally, Anderson localization of light has not yet been observed in $3D$. Even from a theoretical point of view, the existence of a critical density implies that a very large number of scatterers are required to overcome finite-size effects in numerical simulations. A consequence of numerical limitations is that localized modes usually present hybrid spatial profiles, with slowly decaying tails [28,37].

In $3D$, for the confinement along the surface, we consider modes with a center of mass closer to the surface than $R/20$ and analyze the mode by using only the atoms in this layer. An example of such a mode is shown in Fig. 4. The surface localization length is obtained by exponential fitting of the mode profile over the atoms j such that $|R - r_j| \leqslant R/20$, using the great-circle distance. The surface atoms farthest from the center of mass and that constitute an overall 0.005% of the mode weight are excluded from the fitting [28].

The obtained ξ_2^s is presented in Fig. 5, as a function of the cloud atomic density—obtained from an average over all localized modes for each density. Similarly to the $2D$ case, the $3D$ ξ_2^s scales with the predicted $2D$ mean-free path along the surface, l_2^s, but scales quite differently from the $3D$ mean-free path l_3. We note that ξ_2^s also scales differently from the $2D$ self-consistent theory formula [34], yet this prediction assumes a weak disorder, an assumption not verified in our simulations [29]. We remark that it was not possible to associate a polarization to the surface modes, when monitoring the orientation of the dipoles. This may be due to the relatively small size of the samples, which can result in

a strong curvature of the surface and prevent a well-defined polarization.

V. DISCUSSION

The model used in this paper has been applied extensively to two-level systems. However, the confinement of light along the surface reported here is similar to whispering gallery modes and is thus expected to also occur with nonresonant dielectric scatterers. The angular localization, on the other hand, is based on the existence of Anderson localization in dimensions $d - 1$ for such materials, an effect that has already been demonstrated for nonresonant dielectric media in dimensions 1 and 2. We therefore expect our findings to also hold for nonresonant scattering media.

Finally, we note that the edge states discussed in this work are present in both the scalar and vectorial models. In this context, the introduction of a magnetic field introduces two effects that may present an interesting interplay: it splits the scattering channels, whose coupling was preventing localization in $2D$ and $3D$ [18,22], and it breaks the time-reversal symmetry, thus favoring the emergence of topological insulators [38]. Combining these two effects may thus allow us to tune the topological properties of edge states in light-scattering systems.

In conclusion, we have shown that, although vectorial light-scattering systems do not feature a transition to Anderson localization, the confinement of light to the surface in strongly scattering samples results in disorder-induced localization along the surface. In two dimensions, where large systems can be simulated, a clear distinction between radial and angular confinements can be monitored, and the associated confinement lengths exhibit scalings in agreement with lower-dimensional scattering. In three-dimensional systems, finite-size effects prevent a refined analysis, yet the scaling of the localization length scales as expected from a two-dimensional theory. Considering the size of the samples used for both experimental and theoretical studies of Anderson localization of light, these boundary modes must be accounted for carefully.

[1] P. W. Anderson, Phys. Rev. **109**, 1492 (1958).

[2] S. He and J. D. Maynard, Phys. Rev. Lett. **57**, 3171 (1986).

[3] H. Hu, A. Strybulevych, J. H. Page, S. E. Skipetrov, and B. A. van Tiggelen, Nat. Phys. **4**, 945 (2008).

[4] J. Billy, V. Josse, Z. Zuo, A. Bernard, B. Hambrecht, P. Lugan, D. Clément, L. Sanchez-Palencia, P. Bouyer, and A. Aspect, Nature (London) **453**, 891 (2008).

[5] G. Roati, C. D'Errico, L. Fallani, M. Fattori, C. Fort, M. Zaccanti, G. Modugno, M. Modugno, and M. Inguscio, Nature (London) **453**, 895 (2008).

[6] S. S. Kondov, W. R. McGehee, J. J. Zirbel, and B. DeMarco, Science **334**, 66 (2011).

[7] G. Semeghini, M. Landini, P. Castilho, S. Roy, G. Spagnolli, A. Trenkwalder, M. Fattori, M. Inguscio, and G. Modugno, Nat. Phys. **11**, 554 (2015).

[8] W.-B. Shi, L.-Z. Liu, R. Peng, D.-H. Xu, K. Zhang, H. Jing, R.-H. Fan, X.-R. Huang, Q.-J. Wang, and M. Wang, Nano Lett. **18**, 1896 (2018).

[9] S. John and M. J. Stephen, Phys. Rev. B **28**, 6358 (1983).

[10] S. John, Phys. Rev. Lett. **58**, 2486 (1987).

[11] A. Z. Genack and N. Garcia, Phys. Rev. Lett. **66**, 2064 (1991).

[12] D. S. Wiersma, P. Bartolini, A. Lagendijk, and R. Righini, Nature (London) **390**, 671 (1997).

[13] F. J. P. Schuurmans, M. Megens, D. Vanmaekelbergh, and A. Lagendijk, Phys. Rev. Lett. **83**, 2183 (1999).

[14] M. Störzer, P. Gross, C. M. Aegerter, and G. Maret, Phys. Rev. Lett. **96**, 063904 (2006).

[15] P. D. García, S. Stobbe, I. Söllner, and P. Lodahl, Phys. Rev. Lett. **109**, 253902 (2012).

[16] T. Sperling, W. Bührer, C. M. Aegerter, and G. Maret, Nat. Photonics **7**, 48 (2013).

[17] E. Abrahams, P. W. Anderson, D. C. Licciardello, and T. V. Ramakrishnan, Phys. Rev. Lett. **42**, 673 (1979).

[18] S. E. Skipetrov and I. M. Sokolov, Phys. Rev. Lett. **112**, 023905 (2014).

[19] L. Bellando, A. Gero, E. Akkermans, and R. Kaiser, Phys. Rev. A **90**, 063822 (2014).

[20] F. Scheffold and D. Wiersma, Nat. Photon. **7**, 934 (2013).

[21] T. Sperling, L. Schertel, M. Ackermann, G. J. Aubry, C. M. Aegerter, and G. Maret, New J. Phys. **18**, 013039 (2016).

[22] C. E. Máximo, N. Piovella, P. W. Courteille, R. Kaiser, and R. Bachelard, Phys. Rev. A **92**, 062702 (2015).

[23] D. Laurent, O. Legrand, P. Sebbah, C. Vanneste, and F. Mortessagne, Phys. Rev. Lett. **99**, 253902 (2007).

[24] S. E. Skipetrov and I. M. Sokolov, Phys. Rev. Lett. **114**, 053902 (2015).

[25] R. H. Lehmberg, Phys. Rev. A **2**, 883 (1970).

[26] T. Hill, B. C. Sanders, and H. Deng, Phys. Rev. A **95**, 033832 (2017).

[27] F. Sgrignuoli, R. Wang, F. A. Pinheiro, and L. Dal Negro, Phys. Rev. B **99**, 104202 (2019).

[28] N. A. Moreira, R. Kaiser, and R. Bachelard, Localization versus subradiance in three-dimensional scattering of light, Europhysics Lett. **127**, 54003 (2019).

[29] S. E. Skipetrov and I. M. Sokolov, Phys. Rev. B **98**, 064207 (2018).

[30] R. Bachelard, P. Courteille, R. Kaiser, and N. Piovella, Europhys. Lett. **97**, 14004 (2012).

[31] H. C. van de Hulst, *Light Scattering by Small Particles* (John Wiley and Sons, New York, 1957).

[32] J. D. Jackson, *Classical Electrodynamics*, 3rd ed. (John Wiley & Sons, New York, 1999).

[33] M. V. Berry and S. Klein, Eur. J. Phys. **18**, 222 (1997).

[34] P. A. Lee and T. V. Ramakrishnan, Rev. Mod. Phys. **57**, 287 (1985).

[35] P. Wölfle and D. Vollhardt, Int. J. Mod. Phys. B **24**, 1526 (2010).

[36] M. Antezza and Y. Castin, Phys. Rev. A **88**, 033844 (2013).

[37] G. L. Celardo, M. Angeli, and R. Kaiser, Localization of light in subradiant Dicke states: A mobility edge in the imaginary axis, arXiv:1702.04506.

[38] M. Z. Hasan and C. L. Kane, Rev. Mod. Phys. **82**, 3045 (2010).